The International Journal of Advanced Manufacturing Technology (2019) 102:957–968
https://doi.org/10.1007/s00170-018-03238-0

ORIGINAL ARTICLE

Toward the temperature distribution on ball bearing inner rings during single-grit grinding

Guangwei Yu[1] · Qing Wang[1] · Zhuoyuan Song[2] · Dangsheng Fang[1] · Yinwei Li[1] · Yuan Yao[1]

Received: 23 August 2018 / Accepted: 14 December 2018 / Published online: 5 January 2019

Abstract
The paper studies the post-grinding temperature distribution on the inner ring of ball bearing 7008C. A grinding model was proposed to calculate the temperature distribution using the finite element method. The grinding process was simplified based on abrasive grain grinding motion. Our calculation takes account of the non-linear variation in physical properties of the bearing material as the temperature changes and the effects of convective heat transfer in the surrounding environment. A rectangular heat source and cyclic loading method were used to simulate the energy input during grinding, and the grinding temperature fields under different processing parameters were obtained. The calculated temperature fields are in good agreement with experimental results. The proposed model was then utilized to analyze the influence of different processing parameters on the temperature distribution, providing a basis for predicting the phase change and analyzing the post-grinding residual stress. Through processing parameter adjustments, the optimal parameter combinations that do not lead to material phase changes were identified. We hope this analysis will shed some light on the optimization of the bearing grinding process.

Keywords Finite element method · Grinding temperature field · Phase change · Residual stress · Grinding process optimization

1 Introduction

Rolling bearings are basic components in mechanical equipment and have a profound influence on the performance and lifetime of mechanical products. It has been found that fatigue failure is one of the primary failure modes of rolling bearings given proper installation and appropriate lubrication conditions [1, 2]. The distribution of the residual stress on the rolling bearing raceway has a significant influence on the bearing's fatigue life. Compared with turning and milling machining, grinding processes are often selected for final machining in the production of precision components [3].

Grinding of bearing rings is a key process to ensure the accuracy of rolling bearing raceways. The temperature of the grinding raceway directly affects the distribution of residual stress. The mechanical deformation of cylindrical grinding can cause compressive residual stress. Removing the unit volume of metal through grinding requires high-energy input, especially for materials that are difficult to machine [4]. During grinding, due to the high rotational speed of the grinding wheel, it is difficult for the grinding fluid to reach the grinding zone. Most of the energy input during grinding is converted to heat. When not diffused to the surrounding environment in time, the generated heat accumulates during the grinding process within the grinding zone, leading to a large temperature gradient. This may affect the properties of the surface and the layers nearby [5]. Thermal deformation and damage of the workpiece will reduce the grinding precision [6]. When the temperature in the grinding zone reaches a certain threshold, tensile residual stress will be generated. It has been shown that, although the tensile residual stress shortens the bearing fatigue life, the compressive residual stress has a positive effect on the bearing fatigue life [7, 8]. This is because that the compressive residual stress not only prevents the initiation of fatigue crack [9], it also suppresses fatigue crack propagation [10].

Given under different grinding parameter settings, the distribution of grinding-induced temperature and the resulting residual stress vary. Due to the complexity of the grinding process, most grinding problems cannot be solved analytically

✉ Qing Wang
wangqingwq56@163.com

[1] School of Mechatronic Engineering and Automation, Shanghai University, 99 Shangda Road, Baoshan District, Shanghai, China

[2] Department of Mechanical Engineering, University of Hawaii at Manoa, Honolulu, HI 96822, USA

[11]. To optimize the grinding process of ball bearings and properly adjust the process settings during production, it is often necessary to perform numerous experiments that demand a huge amount of human resources, materials, and other related overhead costs. Therefore, establishing a proper grinding model for ball bearings based on finite element methods is of great importance to many aspects of bearing production including optimizing the machining parameters, ensuring the grinding efficiency, controlling the grinding temperature, and minimizing the tensile residual stress.

Several studies exist for mathematically modeling the grinding process and identifying the leading factors of the grinding temperature distribution and residual stress. Jaeger [12] proposed the theory of moving heat source in 1942. He argued that the short and intense energy inputs caused by the interactions between abrasive particles and the workpiece can be assumed to move along the workpiece surface at the same speed of the workpiece. With a uniform ribbon heat source, the temperature distribution can be obtained by integrating the heat source. In 1964, Bei [13] proposed the theory of the triangular heat source model and verified the rationality of the theory. From 1996 to 1997, Rowe et al. [14–16] combined four heat transfer methods for grinding heat to obtain a more accurate model. Several other models have also been proposed based on various heat source settings, including tilted moving heat source [17], high efficiency deep grinding heat source [18], circular arc heat source [19], parabolic heat source [20], and quartic function curves heat source [21], leading to the temperature field models that are much closer to the actual grinding situation.

Most existing research focused on plane grinding. However, few have addressed grinding of curved surfaces, especially for ball bearing. Based on the principle of heat transfer and the finite element method, a grinding model of inner ring of ball bearing 7008C is presented in the ANSYS parametric design language. Our proposed model fully considers the influence of speed of grinding wheel, workpiece speed, grinding depth, grinding fluid, and grinding force. The post-grinding temperature field is obtained with this approach, providing a basis for analyzing the machining quality of bearings.

2 Grinding temperature field of ball bearings

2.1 Heat flux of ball bearing grinding process

To establish a reasonable temperature field model, it is necessary to identify the proper processing parameters and obtain the boundary conditions that are consistent with the actual conditions. As shown in Fig. 1, heat flows into the workpiece, resulting in an increase of the surface temperature [22]. Therefore, it is crucial to obtain the total energy input and

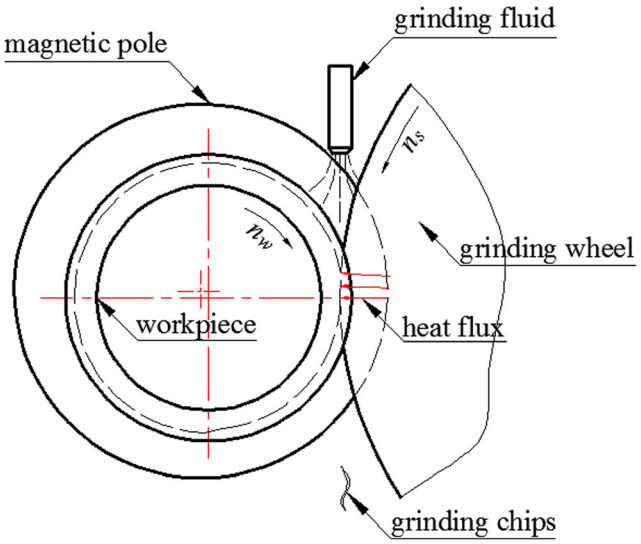

Fig. 1 Schematic diagram of the inner ring grinding model

the heat input ratio of the workpiece during grinding. Power loss during grinding is a major source of grinding heat [23, 24]. According to the conservation of energy, grinding energy is introduced in the forms of radiation and heat to the workpiece, grinding wheel, grinding fluid, and grinding chips.

The following relationship can be obtained:

$$q_t = \frac{F_t \cdot V_s}{b \cdot l_g} \tag{1}$$

$$q_t = q_w + q_{ch} + q_f + q_s + q_u \tag{2}$$

where q_t is the total heat flux; F_t is the tangential grinding force; V_s is the linear speed of wheel; l_g is the contact arc length between the workpiece and the grinding wheel; b is the workpiece width; q_w is the heat flux into the workpiece; q_{ch} is the heat flux into the grinding chips. q_f is the heat flux into the grinding fluid; q_s is the heat flux into the grinding wheel; and q_u is the radiant heat flux. The contact arc length can be obtained through:

$$l_g = \sqrt{d_s \cdot a_p} \tag{3}$$

where d_s is the diameter of the grinding wheel. The heat flux q_{ch} of the chips can be calculated as [20]:

$$q_{ch} = e_{ch} \cdot \frac{b \cdot a_p \cdot V_w}{b \cdot l_g} = \rho_w \cdot c_w \cdot T_{mp} \cdot \frac{a_p \cdot V_w}{l_g} \tag{4}$$

where e_{ch} is the extreme grinding chip energy, which is the thermal energy when the grinding material is about to melt; a_p is the grinding depth; V_w is the linear speed of the workpiece; ρ_w is the density of the workpiece material; c_w is the specific heat capacity of the workpiece material; and T_{mp} is the workpiece material melting point temperature.

During the grinding process, the rotational speed of the grinding wheel is high; therefore, it is difficult for the grinding

fluid to reach the machining surface, and the amount of heat dissipated by the grinding fluid is particularly small; the effect of radiation during grinding is small, and the influence of radiation is negligible. To reflect this, in our calculation, it is assumed that $q_f = 0$ and $q_u = 0$. According to Hahn's model, the heat distribution ratio R_{ws} [25] can be obtained as:

$$R_{ws} = \frac{q_w}{q_w + q_s} = \left[1 + \frac{0.974kg}{(k\rho c)_w^{0.5} \cdot r_0^{0.5} \cdot Vs^{0.5}}\right]^{-1} \tag{5}$$

where k_g is the thermal conductivity of abrasive grain; $(k\rho c)_w^{0.5}$ is the effusivity of the workpiece material [26]; r_0 is the effective contact radius of the grinding wheel grit, which is set to 15 μm [27]. With the above formulas, the heat flux into the bearing can be obtained as:

$$q_w = \frac{q_w}{q_w + q_s} \cdot \left(q_t - q_{ch} - q_f - q_u\right) \tag{6}$$

2.2 Equivalent transformation of grinding parameters of ball bearings

The derivation in Section 2.1 is derived based on the plane grinding theory. Nonetheless, the machining of the inner ring of the ball bearing is a curved-surface grinding process. Therefore, the grinding parameters of the bearing ring must be equivalently projected to the planar grinding model.

As shown in Fig. 1, the grinding of the inner ring is centerless; the workpiece and the grinding wheel rotate simultaneously. As a result, the relative rotational speed and processing time of the bearing should be considered in the calculation. During down-grinding, one has:

$$n_r = n_s - n_w \tag{7}$$

$$T = \frac{1}{n_r} \tag{8}$$

where n_r is the relative rotational speed between the grinding wheel and the bearing ring, n_s is the rotational speed of the grinding wheel, n_w is the rotational speed of bearing, and T is the processing time. The linear speed of wheel, V_s, and the linear speed of bearing, V_w, can be calculated from Eqs. (9) and (10), respectively:

$$V_s = \frac{\pi d_s n_s}{60} \tag{9}$$

$$V_w = \frac{\pi d_w n_w}{60} \tag{10}$$

When grinding the surface, the contact arc length l_g should be converted to the corresponding contact angle θ.

$$\theta = \frac{180 l_g}{\pi r} \tag{11}$$

Then, the heat flux function used in the simulation can be calculated from Eqs. (1)–(11) as Eq. (12). The schematic diagram of the grinding temperature modeling process is shown in Fig. 2.

$$q_w = \left[1 + \frac{0.974k_g}{\sqrt{(k\rho c)_w \cdot r_0 \cdot \left(\pi \frac{\pi d n_s}{60}\right)}}\right]^{-1} \cdot \left[\frac{F_t \cdot \left(\frac{\pi d n_s}{60}\right)}{b \cdot \sqrt{d_s \cdot a_p}} - \rho_w c_w T_{mp} \frac{a_p \cdot \left(\pi \frac{\pi d n_w}{60}\right)}{\sqrt{d_s \cdot a_p}}\right] \tag{12}$$

2.3 Modeling of the ball bearing grinding temperature field based on abrasive grain grinding motion

The grinding depth of the ball bearing ring is generally small, so the grinding surface and the unground surface of the raceway can be considered as the same surface in modeling, and the inclination of the grinding wheel is omitted. Because the grinding of rolling bearing rings is a three-dimensional machining process, three-dimensional thermal units and models should be adopted.

In this paper, the ANSYS parametric design language is used to model and characterize the grinding process. Bearing ring temperature field calculation flowchart is shown in Fig. 3.

1. Selection of unit types

The unit type is Solid90, which is a three-dimensional hexahedral thermal unit suitable for simulating surface boundaries.

2. Definition of material properties

During grinding, the grinding temperature of the bearing rings will increase with the grinding time, and the performance of the workpiece material of the bearing will also change as the temperature increases. When defining physical properties such as material temperature, density, and specific heat capacity, the nonlinear relationship between material and temperature should be considered, and the values of the physical properties of the material at different temperatures should be provided as inputs. The accuracy of the parameters used in our simulation will affect the accuracy of the simulation results to a certain extent. Considering that the material property data reported by Shen et al. [26] have been widely adopted in

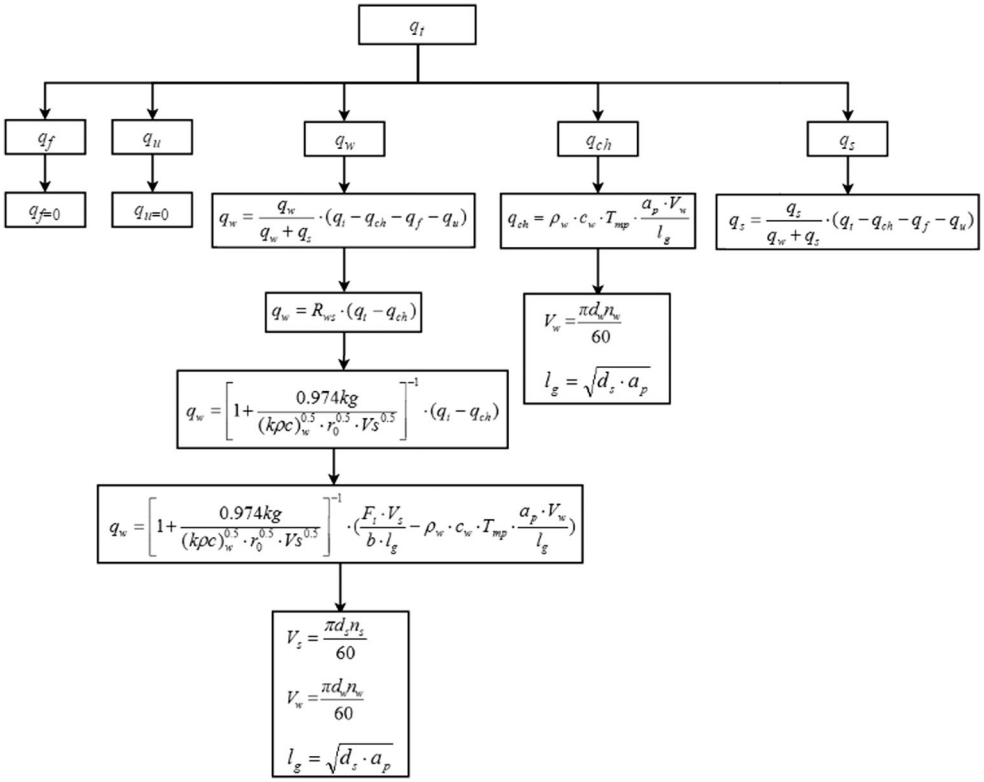

Fig. 2 The schematic diagram of the grinding temperature modeling process

multiple related research (e.g., [28]), we refer to Shen's data for this study. The temperature performance of the material of the bearing ring GCr15 at different temperatures is shown in Table 1.

3. Model creation and discretization

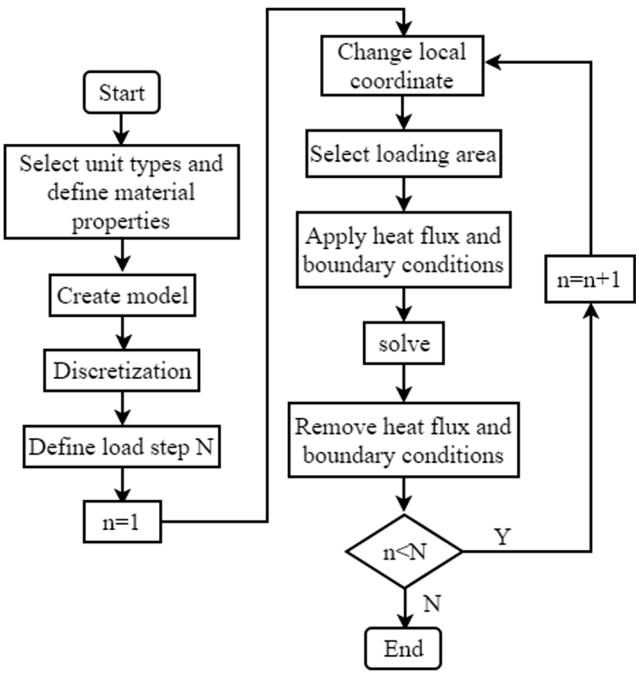

Fig. 3 Flowchart of the calculation of the bearing ring grinding temperature field

The grinding model is created according to the dimensions of the inner ring of ball bearing 7008C. The resolution of the mesh grid can have a great influence on the accuracy of the results and the computational time. During grinding, the temperature gradient near the bearing raceway is large, while the temperature gradient away from the surface of the grinding zone is relatively low. When the mesh is too coarse, it may be difficult to capture the temperature change on the grinding surface, leading to a large modeling error. On the other hand, when the grid is too dense, the computation accuracy will be improved at the cost of longer computation time. Therefore, different mesh densities should be used for different temperature gradients during discretization. A finer mesh should be used near the grinding raceway, and a sparser mesh should be used for regions away from the raceway. In this way, the calculation efficiency can be improved while ensuring the accuracy. After meshing, the number of grids in the circumferential direction of the bearing is 100, the total number of units is 7500, and the total number of nodes is 36,200. The dimension of the 7008C inner ring is shown in Table 2 and the model after meshing is shown in Fig. 4.

4. Boundary conditions and initial temperature

The boundary conditions for bearing grinding vary with the grinding position. During dry grinding, the thermal conductivity of air is low, therefore the thermal convection of the air is negligible. During wet grinding, grinding fluid will reduce the grinding temperature [29] and thermal convection conditions

Table 1 Temperature performance values of GCr15 at different temperatures [26]

Temperature (°C)	Thermal conductivity (W/(m·°C))	Density (kg/m^3)	Specific heat capacity (J/kg·°C)
25	49.68	7850	460
100	46.89	7830	490
200	43.56	7800	530
300	40.73	7760	565
400	38.12	7730	608
500	36.31	7690	657
700	32.58	7630	726

are used to simulate the cooling effect of the grinding fluid. According to Jin et al. [30], the convective heat transfer coefficient is 82,000 W/m^2·K. Since it is difficult for the grinding fluid to reach the grinding zone, convective boundary conditions of the grinding fluid are applied to the non-grinding portion of the bearing raceway in our model. Since the grinding of the bearing raceway is centerless and one of the end faces of the bearing is axially fixed by the magnetic pole, adiabatic boundary conditions are applied to the end face. The initial temperature of the bearing inner ring is assumed to be 20 °C. The boundary conditions and initial temperature applied in the model are shown in Fig. 5.

5. Simplification of the grinding process based on abrasive grain grinding motion and the application of heat flux

The grinding process of the grinding wheel can be considered as abrasive grain sliding, plowing, and cutting. During grinding, each abrasive grain can be considered as a point heat source, and the combination of all abrasive grains under the entire contact arc can be treated as a surface heat source. The grinding process can be considered as the movement of the surface heat source on the raceway. Therefore, the surface heat source should be loaded to the grinding zone, and the application position should change with time. The surface heat source is the heat flux into the workpiece as mentioned in Section 2. The heat flux function used in the simulation is described in Eq. (12) of Section 2.2. At a given time step, the distribution of the heat flux function is shown in Fig. 5, the direction of which is perpendicular to the raceway surface.

Table 2 7008C bearing inner ring size

Internal diameter (mm)	Inner channel diameter (mm)	Maximum thickness (mm)	Minimum thickness (mm)	Width (mm)
40	7.98	4.9	3.485	15

The moving heat source cannot be directly applied in ANSYS. Therefore, a small-spacing, iterative approach is adopted to apply the heat source. The heat flux is applied to the grinding zone during a short period of time iteratively. When the value of heat flux changes, it is necessary to change the local coordinate accordingly to simulate the movement of the heat source. The grinding area is selected to apply the heat flux through arrays and functions in ANSYS. Upon the completion of one iteration of calculation, the heat flux applied in the grinding zone must be removed, and the temperature calculated at this stage is used as the initial condition for the next stage. In such a way, the movement of the heat source and the transient temperature field of the grinding process can be accurately simulated. During calculation, the time step should be selected appropriately to ensure both simulation efficiency and accuracy. The total grinding time can be calculated according to Eqs. (7)–(11). The contact arc length should be converted to the corresponding contact angle θ in order to properly apply the heat flux. The time steps are determined based on the time stamps of the contact angles, and each time step is further divided into three intervals.

The diameter of the grinding wheel is 500 mm and ambient temperature is 20 °C. The grinding parameters of the bearing ring are shown in Table 3.

The grinding force of per unit width is 0.747 N/mm, and the calculation parameters can be calculated by Eqs. (1)–(6), as shown in Table 4.

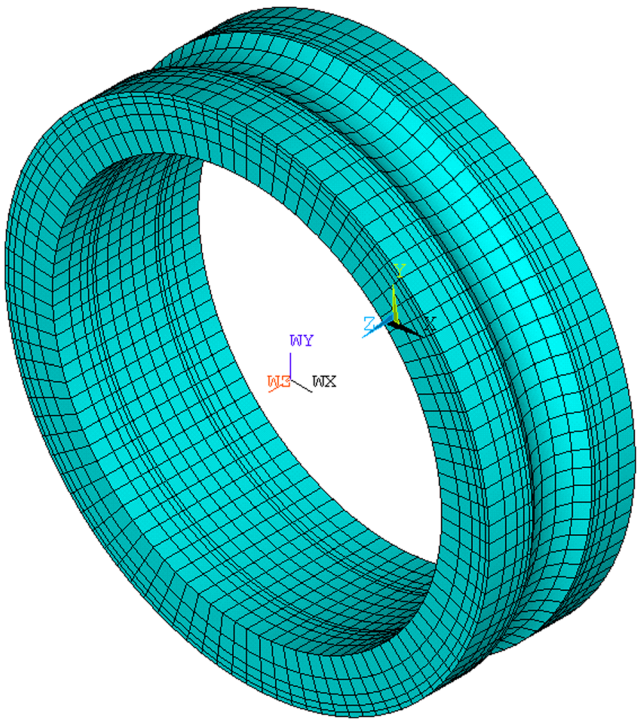

Fig. 4 Discretized model of the bearing ring

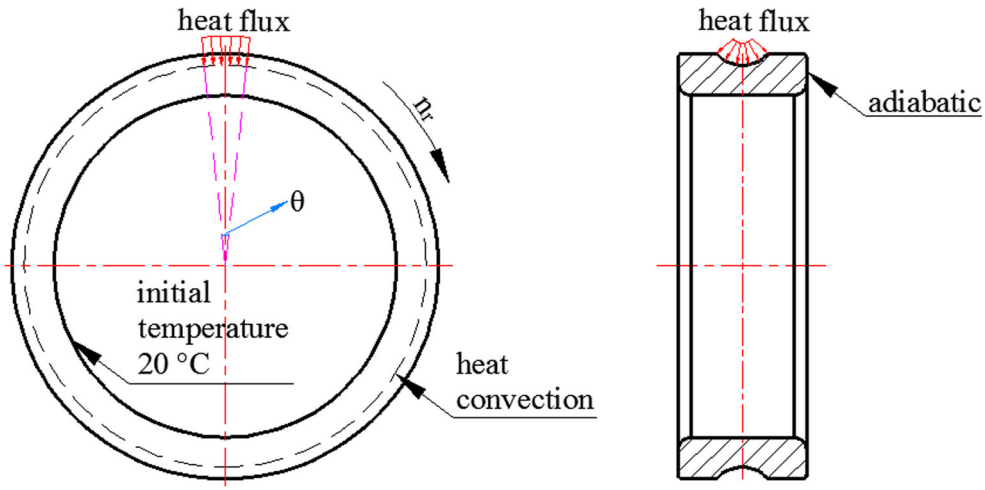

Fig. 5 Schematic diagram of heat flux loading and boundary conditions

3 Calculation results

Based on the grinding parameters in Table 3, the temperature field distribution of the inner ring can be calculated as shown in Fig. 6, where the location, the magnitude of the temperature, and the maximum temperature of the bearing raceway at 0.0128 s are shown. It can be seen from Fig. 6 that the maximum grinding temperature of the bearing ring at 22nd time step is 320 °C.

In this simulation, the intersection of the positive x-axis direction and the raceway surface is considered to be the starting location of the grinding process. The grinding direction is counterclockwise. At the 22nd time step, the path is defined on the bearing raceway surface from the starting point of grinding along the grinding direction, and the temperature result is mapped onto the path. Figure 7 shows the temperature changes at different locations on the raceway surface. The abscissa is the distance between the points on the raceway from the starting point of grinding, and the ordinate is the instantaneous temperature. According to Fig. 7, the maximum temperature is approximately 320 °C at the 22nd time step. The distance between the grinding position and the starting point of grinding is approximately 0.01 m. Temperature at both ends far away from the grinding zone gradually approaches the ambient temperature.

At the 22nd time step, the path is defined from point A on the edge of the bearing raceway (Fig. 6) to the bearing's center away from the grinding surface. The temperature distribution is mapped onto the path. Figure 8 shows the temperature changes of the bearing at different depths. The abscissa is the distance from the grinding surface of the bearing, and the ordinate is the temperature at the current time. As can be seen in Fig. 8, the closer it is from the grinding surface, the higher the grinding temperature will be and vice versa. Temperature far away from the grinding zone gradually approaches the ambient temperature.

The angle of grinding position relative to the starting point of grinding is denoted by β. Figure 9 shows the temperature variation on the bearing raceway surface at different positions over time during the grinding process. The position of the bearing is indicated by the rotation angle β. During the grinding process, since the contact location between the grinding wheel and the bearing is constantly changing, the location of the heat source is varying. Therefore, the position of the highest temperature in the grinding area is also changing. Figure 9 shows the temperature changes of the bearing raceway from the angle of 7.2 to 28.8°. The grinding temperature at each location of the bearing increases rapidly and then decreases gradually. When the workpiece temperature is close to ambient temperature, its variation is slow. Since dissipation conditions are the same, the rate of temperature variation at all locations is identical. At the beginning of grinding, the temperature of the grinding zone is low. During the process of grinding, the grinding heat accumulates, and the maximum grinding temperature is constantly rising due to the untimely heat dissipation and the influence from the heat source. When grinding to the angle of approximately 21.6°, the maximum

Table 3 Grinding parameters of bearing ring

Grinding wheel	Workpiece material	Grinding method	Rotational speed of grinding wheel	Rotational speed of workpiece
A80L6V	Gcr15	Wet grinding	2300 r/min	240 r/min

Table 4 Calculation parameters of bearing ring grinding

l_g	q_t	q_{ch}	q_w	R_{ws}
1 mm	44.98 W/mm^2	6.81 W/mm^2	35.04 W/mm^2	91.81%

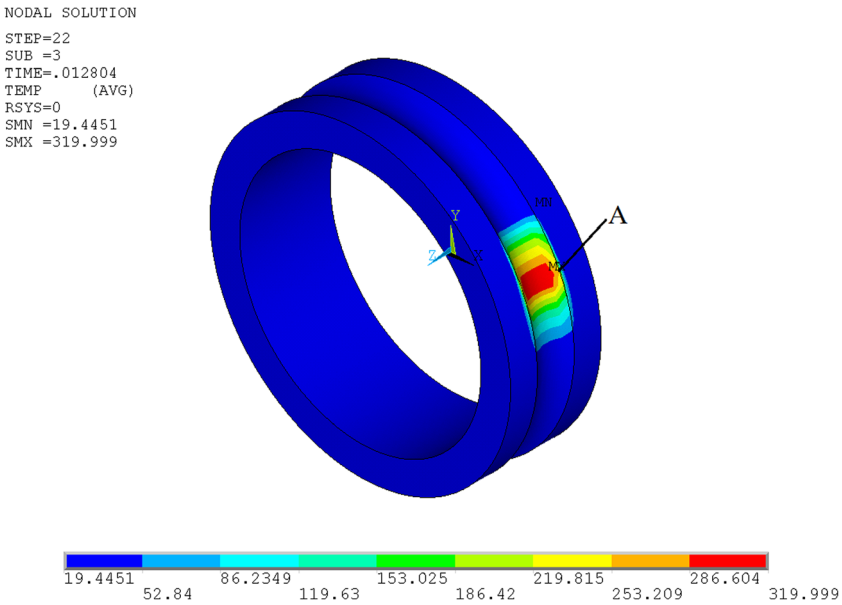

Fig. 6 Distribution of temperature field

temperature gradually stabilizes, and the maximum temperature reaches approximately 320 °C. During the subsequent grinding process, the maximum temperature is nearly constant, which is consistent with our observation during actual grinding processes.

4 Experimental verification

4.1 Temperature measurement system and verification

It is essential to carry out temperature measurement tests to verify the reliability of our simulation results. The maximum grinding temperature is one of the most critical temperatures during grinding. It can be used to evaluate whether the workpiece will produce tensile residual stress or undergo phase transition after grinding. Therefore, it is necessary to measure the maximum temperature during grinding. When grinding the bearing raceway, the surface being grinded is a concave curved surface and the maximum temperature is at the midpoint of the raceway. Therefore, the temperature measurement system needs to measure the temperature at that position.

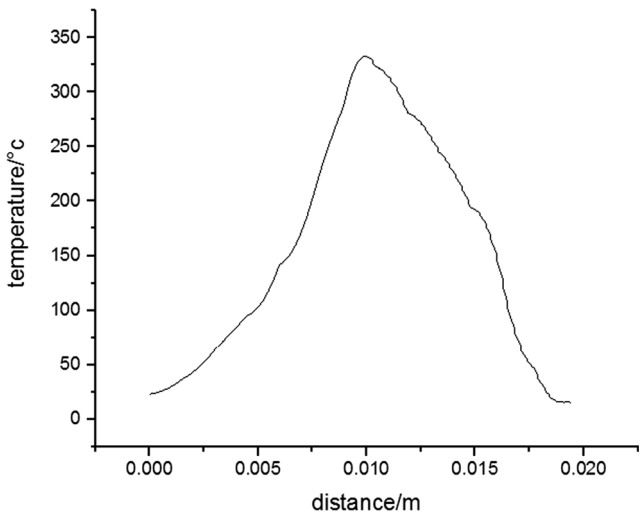

Fig. 7 Temperature distribution at different locations on the raceway surface

There are two common methods for measuring the temperature of bearing grinding process, namely, the thermocouple method and the infrared thermography method. It is quite difficult to measure the grinding temperature of curved surfaces. When grinding the bearing's inner ring, the contact area is larger than that of plane grinding. The grinding wheel blocks the grinding zone, and the coolant and dust of the chips will affect the accuracy of infrared temperature measurement. Therefore, the temperature of the contact zone often cannot be directly measured by the infrared thermography method [31].

Wang [21] proposed a special thermocouple method to experimentally measure the temperature of the bearing inner ring during grinding. The schematic diagram of temperature measurement system is shown in Fig. 10. As shown in Fig. 10, a blind hole is drilled on the inner wall of the bearing inner ring. The distance between the end of blind hole and the surface of bearing raceway must be less than 0.5 mm. The constantan wire and the steel wire are inserted into the blind hole to form a contact with the wall of the hole. The two wires are then fixed in the blind hole through super glue to form a thermocouple joint. When the temperature of thermocouple junction changes, thermocouple converts the temperature signal into an electrical signal, which can be derived from the constantan wire

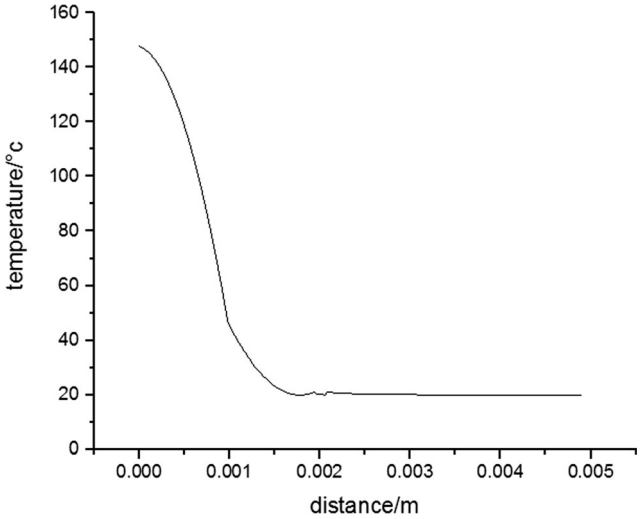

Fig. 8 Temperature variation at different depths

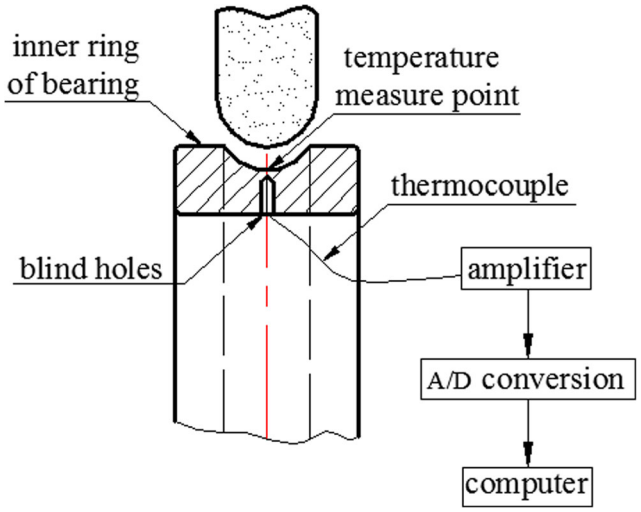

Fig. 10 Schematic diagram of the temperature measurement system proposed by Wang [21]

and steel wire. After signal amplification and A/D conversion, the temperature of measuring point can be transmitted to the computer.

Using this method, the maximum experimental temperature under the conditions discussed in Section 3 is 315.8 °C [21], while the maximum grinding temperature is 320 °C. The modeling error is 1.3%, proving the validity of the model.

4.2 Effect of different processing parameters on grinding temperature

According to the model presented in the previous section, calculation results of the maximum grinding temperature under different parameters are obtained. A comparison between the calculation results of the maximum grinding temperature under different parameters and the experimental results [21] is shown in Table 5.

The error between the experimental results and the calculated results is 1.3%, and the maximum error is 10%.

4.2.1 Effect of different rotational speeds of workpiece on grinding temperature

The influence of rotational speed of workpiece on grinding temperature can be obtained by comparing the experimental data of groups 5, 6, and 7 in Table 5. As shown in Fig. 11, results of the temperature distribution show that the maximum grinding temperature increases with the rotational speed of the workpiece under this grinding setting. That is, the grinding temperature does not necessarily decrease as the rotational speed of the workpiece increases. This is because the process of grinding is also affected by other factors. On the one hand, when the rotation speed of the grinding wheel increases, the action time of the grinding wheel abrasive particles on the workpiece decreases. Grinding fluid and abrasive debris carry away relatively more heat and lower the grinding temperature. On the other hand, because the grinding force is proportional to the linear speed of workpiece, the grinding force will increase as the rotational speed of the grinding workpiece increases. It can be seen from Eq. (6) that the energy delivered to

Fig. 9 Temperature variation of bearing raceways at different locations over time

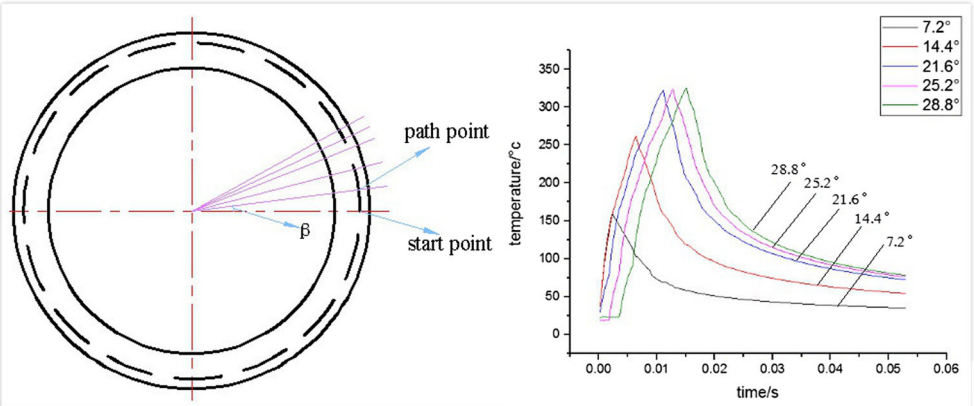

Table 5 Comparison of calculated and experimental values of maximum grinding temperature

Group	n_s (r/min)	n_w (r/min)	a_p (μm)	Experimental values (°C)	Calculated values (°C)	Error (%)
1	2300	120	1	118.2	112.8	−4.6
2	2300	180	1	132.8	144.3	8.7
3	2300	120	1.5	167.4	151.8	−9.3
4	2300	180	1.5	200.5	213.8	6.6
5	2300	120	2	217.5	195.7	−10
6	2300	180	2	263.1	255.0	−3.4
7	2300	240	2	315.8	320.0	1.3

the workpiece (heat flux) during grinding increases, and the increase of heat flux increases the grinding temperature. Experiments show that high-frequency vibrations are common when the rotational speed of the workpiece is too high, and they are often accompanied by vibration burn (point burn) [32]. Therefore, when the effect of heat flux dominates, the grinding temperature will rise, and the temperature decreases otherwise.

4.2.2 Effect of different grinding depths on grinding temperature

The influence of grinding depth on grinding temperature can be obtained by comparing the experimental data of groups 2, 4, and 6 in Table 5. As shown in Fig. 12, the speed of the grinding wheel of the three groups of data is 2300 r/min, the rotational speed of workpiece is 180 r/min, and grinding depths of the workpiece are 1 μm, 1.5 μm, and 2 μm, respectively. By comparing the temperature results, it can be seen that the maximum grinding temperature increases with the grinding depth. As the depth of grinding increases, the grinding force also increases; the energy delivered to the workpiece during grinding (i.e., heat flux) increases. Increasing the grinding speed of the workpiece appropriately and reducing the grinding depth will help to reduce the grinding temperature of the bearing.

4.3 Effect of grinding temperature on processing quality

High grinding temperature can cause surface burn, dimension deviation, and surface deterioration. They also have a significant influence on the fatigue life of the workpiece. When the temperature reaches the transformation temperature, the workpiece will undergo phase transition, and the strength and hardness of the workpiece will change. When the temperature is too high, the workpiece may produce tensile residual stress, which will reduce the fatigue life of the bearing. Therefore, if the phase transition temperature of the material is known and the bearing temperature is estimated by the proposed finite element method, the phase change of the workpiece can be evaluated, and the influence of the grinding temperature on the machining quality can be predicted.

In 1984, Gui et al. [33] used optical metallography, microhardness tester, X-ray diffraction, electron

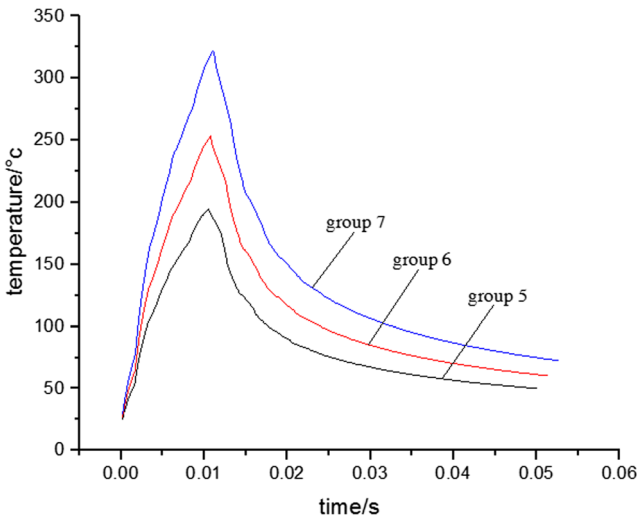

Fig. 11 Influence of the rotational speed of the workpiece on the grinding temperature

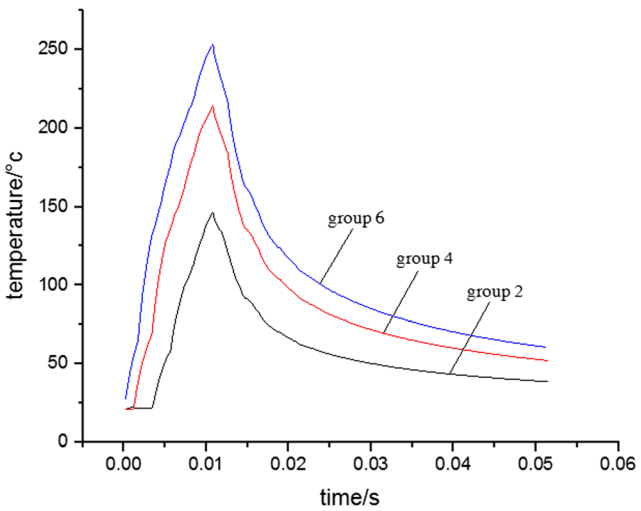

Fig. 12 Effect of grinding depth on grinding temperature

microscope, electron probe, electron energy analyzer, and isotope wear test to study the modification layers of GCr15 steel in different grinding processes. As shown by the test results, when the grinding temperature of heat-treated GCr15 steel is higher than the tempering temperature, the workpiece will be tempered, and the hardness and wear resistance of the workpiece will be reduced. When the grinding temperature is higher than Ac1, which is the temperature at which austenite begins to form during heating, austenite will be generated in a local area of the workpiece. Subsequently, if the region is cooled by the grinding fluid, the double-quenched martensite will be produced, which will increase the internal stress and reduce the contact fatigue strength of the workpiece. It is known that the tempering temperature of GCr15 steel is 160~180 °C [34], the martensite transformation temperature (starting temperature of martensite transformation) is 235 °C, the Ac1 of GCr15 steel is 745 °C, and the Accm temperature (austenitizing temperature) of GCr15 steel is 900 °C. The 7th group of data shows that the maximum grinding temperature is approximately 320 °C, that is, the parameters of the group reached the martensite transition temperature and the transformation of martensite occurred. The tempering phenomenon occurred in some regions, so the strength and hardness value decreased. However, the austenite transformation and double-quenched martensite transformation did not occur.

In 2014, Fergani et al. [35] established a physics-based model through rigorous derivations. The model can predict the onset grinding temperature of tensile residual stress of hardened bearing steel AISI521000. The accuracy of the model is verified by subsequent X-ray and neutron diffraction measurement. The comparison of onset temperature between simulation results and experimental results was shown in Fig. 13. The diagram shows that results of Fergani's model were in good agreement with the experimental results. The model can be used to predict the critical temperature of tensile residual stress of hardened steel AISI521000. The onset temperature of hardened bearing steel AISI521000 for both grinding and traverse directions is approximately 190 °C. Because the mechanical properties of the hardened bearing steel AISI521000 and the hardened bearing steel Gcr15 are similar, it is known that under the 7th group of experimental parameters, the tensile residual stress on the bearing raceway surface has been generated, and the fatigue life of the bearing has been reduced.

According to the data groups of 1 and 2 in Table 5, it can be found that when the rotational speed of grinding wheel is 2300 r/min and the grinding depth of the workpiece is 1 μm, the tensile residual stress will not be produced. According to the data groups 3 and 4, the tensile residual stress has been produced when the rotational speed of grinding wheel is 2300 r/min, the grinding depth of the workpiece is 1.5 μm, and the rotational speed of workpiece is 180 r/min. Therefore, in combination with the rotational speed of grinding wheel and the grinding depth parameters, the rotational speed of the grinding wheel should be less than 180 r/min to minimize or even eliminate the generation of tensile residual stress. According to the data groups of 5, 6, and 7, the tensile residual stress has been generated when the rotational wheel speed is 2300 r/min, the workpiece depth is 2 μm, and the rotational speed of workpiece is 120 r/min. Therefore, in combination with the parameters of the rotational speed of grinding wheel and grinding depth, the rotational speed of workpiece should be less than 120 r/min to minimize or even eliminate the generation of residual stress.

5 Conclusions

Based on the principle of heat transfer and finite element analysis, a grinding model of the ball bearing 7008C inner ring is presented. In the proposed model, the grinding process is simplified as the abrasive grain grinding motion with grinding fluid. The grinding temperature field and the limiting temperature under working conditions can

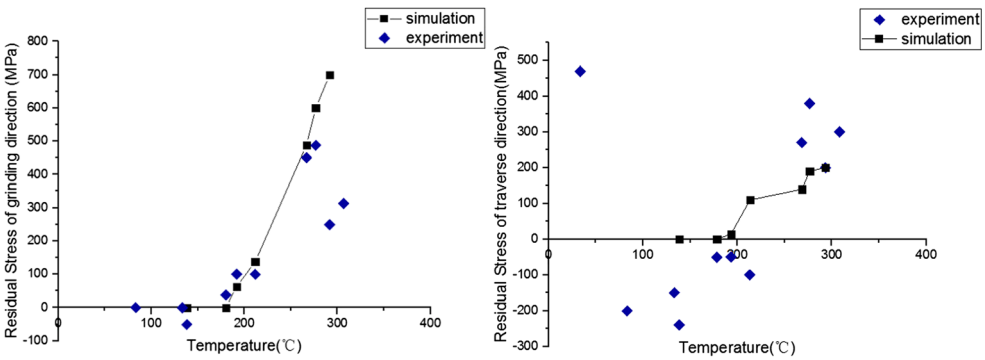

Fig. 13 Comparison of onset temperature between simulation results and experimental results from [35]

be simulated by processing parameters such as grinding depth, workpiece speed, and grinding fluid. It is found that the proposed simulation method is in good agreement with the experiments.

The effect of different parameters on the grinding temperature is analyzed. Results show that the grinding temperature can be reduced to a certain extent by improving the grinding speed and reducing the grinding depth of the workpiece while ensuring the quality of the bearing grinding. However, when the speed of the workpiece is too high, it is likely to cause vibration burn. The increase in workpiece speed does not necessarily reduce the grinding temperature. Therefore, the workpiece speed must not be excessively increased.

According to the phase change temperature of bearing steel and the starting temperature of tensile residual stress, the proposed grinding model can be utilized to determine whether the phase change of the workpiece occurs and whether the tensile residual stress is produced. The influence of the grinding temperature on the processing quality can be predicted in such a way, which is of practical significance for the optimization of the processing technology of bearings.

References

1. Liu SX, Lu YF (2001) Life test and failure analysis on site for super precision high speed spindle bearing. Bearing 6:36–37. https://doi.org/10.3969/j.issn.1000-3762.2001.06.019
2. Wang Y (2009) Failure of rolling bearing in industrial motors. Electric Mach Control Appl 36(9):38–43. https://doi.org/10.3969/j.issn.1673-6540.2009.09.010
3. Wang X, Yu T, Sun X, Shi Y, Wang WS (2016) Study of 3D grinding temperature field based on finite difference method: considering machining parameters and energy partition. Int J Adv Manuf Technol 84(5–8):1–13. https://doi.org/10.1007/s00170-015-7757-z
4. Li BK, Li CH, Zhang YB, Wang YG, Yang M, Jia DZ, Zhang NQ, Wu QD, Ding WF (2017) Numerical and experimental research on the grinding temperature of minimum quantity lubrication cooling of different workpiece materials using vegetable oil-based nanofluids. Int J Adv Manuf Technol 93(5–8):1971–1988. https://doi.org/10.1007/s00170-017-0643-0
5. Mamalis AG, Kundrák J, Manolakos DE, Gyani K, Markopoulos A, Horvath M (2003) Effect of the workpiece material on the heat affected zones during grinding: a numerical simulation. Int J Adv Manuf Technol 22(11–12):761–767. https://doi.org/10.1007/s00170-003-1685-z
6. Zhou L, Huang ST, Zhang CY (2013) Numerical and experimental studies on the temperature field in precision grinding of SiCp/Al composites. Int J Adv Manuf Technol 67(5–8):1007–1014. https://doi.org/10.1007/s00170-012-4543-z
7. Hu NS, Wang QY, Lin L, Tao Y (1992) Prediction of fatigue short crack growth rate in compressive residual stress field. J Xi'an Jiaotong Univ 3:93–98 (in Chinese)
8. He JW, Hu NS, Zhang DQ (1992) Effect of residual stress on high cycle fatigue performance. J Xi'an Jiaotong Univ 3:25–32 (in Chinese)
9. Choi Y, Liu CR (2006) Rolling contact fatigue life of finish hard machined surfaces: part 1 model development. Wear 261(5):485–491
10. Choi Y (2009) A study on the effects of machining-induced residual stress on rolling contact fatigue. Int J Fatigue 31(10):1517–1523
11. Zhou LQ, Li YP, Chen ZG (2009) Thermal deformation simulation for an internal grinding cirque by finite element method. Mod Mach 43(5–6):455
12. Jaeger JC (1942) Moving sources of heat and the temperature of sliding contacts. J Procroysoc NSW 76:203–224
13. Bei JY (1964) Analysis and study of grinding temperature. J Shanghai Jiaotong Univ 3:57–73 (in Chinese)
14. Rowe WB, Black SCE, Mills B, Morgan MN, Qi HS (1997) Grinding temperatures and energy partitioning. Proc Math Phys Eng Sci 453(1960):1083–1104
15. Rowe WB, Morgan MN, Black SCE, Mills B (1996) A simplified approach to control of thermal damage in grinding. CIRP Ann Manuf Technol 45(1):299–302
16. Rowe WB, Black SCE, Mills B (1996) Analysis of grinding temperatures by energy partitioning. Proc Inst Mech Eng B J Eng Manuf 210(62):579–588
17. Cai GQ, Zheng HW (1985) Some experimental studies on the grinding temperature of steel bille. J Northeast Univ Nat Sci 4:77–82 (in Chinese)
18. Zhao HH, Feng BF, Jin T, Cai GQ (2003) Three analytical heat models for high efficiency deep grinding. Diamond Abras Eng 2:18–20. https://doi.org/10.3969/j.issn.1006-852X.2003.02.005
19. Zhang L (2006) Theoretical analysis and experimental study on single plane grinding hardening technology. Dissertation, Shandong University (in Chinese)
20. Mao C (2008) Study of temperature field and thermal damage in plane grinding. Dissertation, Hunan University (in Chinese)
21. Wang DX (2015) Study on residual stress of roller bearing inner ring raceway grinding. Dissertation, Shandong University (in Chinese)
22. Salonitis K (2017) A hybrid cellular automata-finite element model for the simulation of the grind-hardening process. Int J Adv Manuf Technol 93(1):1–7. https://doi.org/10.1007/s00170-017-0829-5
23. Chen X, Rowe WB, Mccormack DF (2000) Analysis of the transitional temperature for tensile residual stress in grinding. J Mater Process Technol 107(1):216–221. https://doi.org/10.1016/S0924-0136(00)00692-0
24. Tong XF (2007) Finite element analysis and simulation of temperature field in grinding zone. Dissertation, Wuhan University of Technology (in Chinese)
25. Hahn RS (1962) On the nature of the grinding process. In: Proceeding of the 3rd International Machine Tool Design and Research Conference. pp 129–154
26. Shen NF, Zhang DJ, Li ZD (2003) New handbook of metallic materials. Science Publishing Company, China (in Chinese)
27. Rowe WB, Black SCE, Mills B, Qi HS, Morgan MN (1995) Experimental investigation of heat transfer in grinding. CIRP Ann Manuf Technol 44(1):329–332
28. Mao C, Zhou ZX, Ren YH, Zhang B (2010) Analysis and FEM simulation of temperature field in wet surface grinding. Adv Manuf Process 25(6):399–406. https://doi.org/10.1080/10426910903124811
29. Parente MPL, Vieira AA, Baptista AM (2012) Experimental and numerical study of the temperature field during creep feed grinding. Int J Adv Manuf Technol 61(1–4):127–134

30. Jin T, Stephenson DJ, Rowe WB (2003) Estimation of the convection heat transfer coefficient of coolant within the grinding zone. Proc Inst Mech Eng B J Eng Manuf 217(3):397–407
31. Jiang JL (2014) Study on surface topography and metamorphic layer of rolling bearing raceway grinding. Dissertation, Shandong University (in Chinese)
32. Anon (1980) Technological test for grinding surface deterioration layer of bearing ring. Bearing 03:38–46 (in Chinese)
33. Gui LF, Tang RJ, Xi BM, Bao WH (1984) Research on grinding steel metamorphic layer of bearing steel. J Mech Eng 20(1):39–50
34. Lu MJ (2004) Handbook of practical mechanical engineering materials. Liaoning Science and Technology Press, China (in Chinese)
35. Fergani O, Shao Y, Lazoglu I, Liang SY (2014) Temperature effects on grinding residual stress. Proc CIRP 14:2–6. https://doi.org/10.1016/j.procir.2014.03.100